FERMILAB-CONF-08-410-AD

LANDAU DAMPING OF SPACE-CHARGE DOMINATED FERMILAB BOOSTER BEAM

K.Y. Ng

Fermilab, P.O. Box 500, Batavia, IL 60510, USA

(September 19, 2008)

Submitted to

HB2008

42nd ICFA Advanced Beam Dynamics Workshop

on High-Intensity, High-Brightness Hadron Beams

Nashville, Tennessee, USA

August 25-29, 2008

LANDAU DAMPING OF SPACE-CHARGE DOMINATED FERMILAB BOOSTER BEAM

K.Y. Ng*, Fermilab†, P.O. Box 500, Batavia, IL 60510, USA

Abstract

The stable region of the Fermilab Booster beam in the complex coherent-tune-shift plane appears to have been shifted far away from the origin by its intense space-charge making Landau damping impossible. However, it is shown that the bunching structure of the beam reduces the mean space-charge tune shift. As a result, the beam can be stabilized by suitable octupole-driven tune spread.

INTRODUCTION

The Fermilab Booster beam has maximum space-charge tune shift of $\Delta\nu_{\rm max}^{\rm spch} \sim 0.5$ near injection and the incoherent tune spread is shifted quite far away from the coherent tune. We wonder why Landau damping coming from octupoles can be possible, because the inductive tune spread of the vacuum chamber cannot be too large. This ambiguity can be resolved when the bunching structure of the beam is considered.

STABILITY CONTOURS

Following the analytic solution of Métral and Ruggiero [1], we computed the stability contour of the Fermilab Booster beam including space-charge and octupole tune spread. The dashed curve in Fig. 1 shows the stability contour of having an octupole tune spread of roughly $-0.042 < \Delta\nu_y < 0.065$ if space-charge is totally neglected. The plot is $\mathcal{R}e\,\Delta\nu_{\rm coh}^y$ versus $\mathcal{I}m\,\Delta\nu_{\rm coh}^y$, which is essentially $-\mathcal{I}m\,Z_1^\perp$ versus $-\mathcal{R}e\,Z_1^\perp$ with $Z_1^\perp$ being the transverse impedance experienced by the beam. The region under the contour implies stability while the region above implies instability. When space-charge is turned on according to the information in Table I, this stability contour becomes the solid red curve with a much wider stability region as a result of the large space-charge tune spread. Unfortunately, this wide stable area has been shifted far far away from the center of the plot. Thus, for the beam to be stable, the inductive part of the vacuum chamber impedance must be extraordinarily large so as to provide an inductive coherent tune shift of at least ~ -0.2. But the inductive impedance has been measured and computed to be very much smaller [2]. Even when the space-charge force is reduced to 50% (green curve), an inductive tune shift of ~ 0.1 is required for stability. We see that stability is restored only when the space-charge is reduced to about 10% (blue curve). In the derivation of the contours, coasting beam with peak beam current has been assumed.

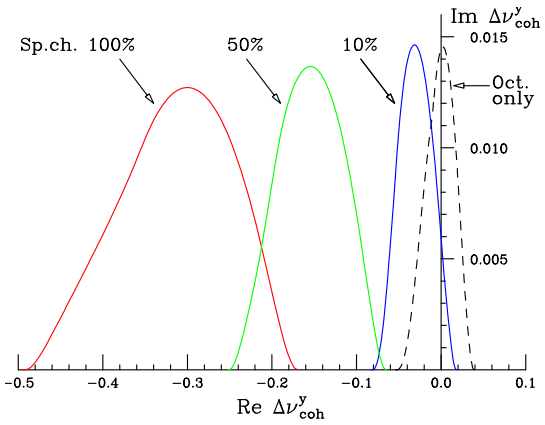

Figure 1: Stability contour from octupole alone shown in dashes changes to the red curve with the introduction of full space-charge force. It changes to the green and blue curves when space-charge is reduced to, respectively, 50% and 10%.

Table I: Some properties of the Fermilab Booster and its beam near injection.

Radius R (m)	75.42
Total Energy E (GeV)	1.40
Rf harmonic	84
Transition gamma γ_t	5.440
Bunch intensity N_b	6×10^{10}
Tune ν_x/ν_y	6.8/6.8
Normalized rms emittance (10^{-6} πm)	2.00
Rms bunch length σ_z (m)	0.70

EFFECTS OF ELECTRON CLOUD

A large buildup of electrons in the beam region can neutralize the proton charge and thus decrease the amount of space-charge tune shifts. The code POSINST [3] is employed to study electron cloud buildup inside the unshielded combined-function F- and D-magnets ($\sim 60\%$ of the ring) and all the adjoining beam pipes ($\sim 40\%$ of the ring) in the Fermilab Booster near injection. We find that

* ng@fnal.gov

† Operated by the U.S. Department of Energy, under contract with the Fermi Research Alliance, LLC.

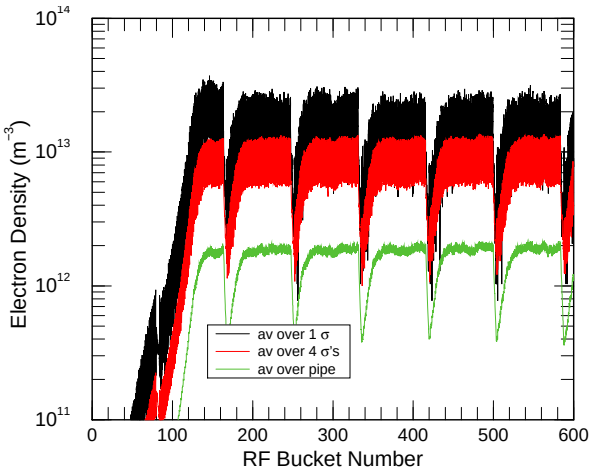

Figure 2: (Color) Electron density inside a D-magnet with SEY=1.6. Black and red curves depict the electron densities averaged over one and four $\sigma_{x,y}$'s of the beam, while the green curve is the electron density averaged over the whole magnet cross section. 81 consecutive bunches and 3 empty buckets are assumed. The dips represent empty buckets or ends of revolutions.

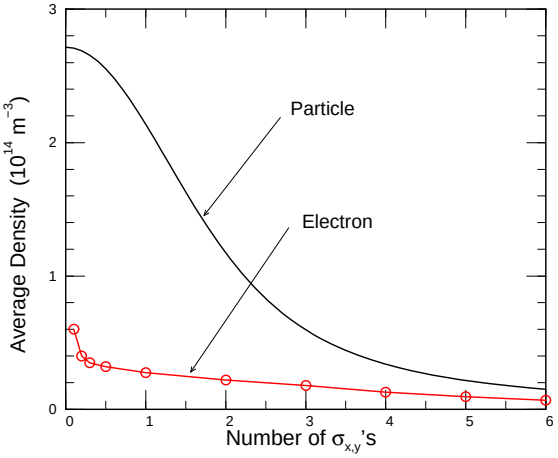

Figure 3: Particle density averaged over n $\sigma_{x,y}$'s is seen to decrease rapidly with n. The corresponding electron density averaged over n $\sigma_{x,y}$'s, although smaller, yet decreases less rapidly.

electron cloud production can reach saturation [4] in the D-magnets when the secondary-emission yield (SEY) ≥ 1.5, while it requires a SEY≥ 1.9 to reach saturation in the F-magnets. For the 168 m of $2.25''$ beam pipe, saturation is reached when SEY≥ 1.6, but for the 28.8 m of beam pipe saturation is reached when SEY≥ 1.5.

Figure 2 shows the electron linear density buildup inside the D-magnet with SEY$=1.6$, where saturation is reached within about 140 rf buckets or less than two revolution turns. But the electron density appears to be very much smaller than the peak beam particle density of $\rho_b^{\rm pk} = N_b/[(2\pi)^{3/2}\sigma_x\sigma_y\sigma_z] = 2.72 \times 10^{14}$ m^{-3}. However, the particle density decreases very rapidly away from the beam axis, but the electron density does not. The particle density averaged over n $\sigma_{x,y}$'s is given by

$$\rho_b(n\sigma_{x,y}) = \rho_b^{\rm pk}\frac{2}{n^2}\left(1-e^{-n^2/2}\right), \qquad (3.1)$$

and is shown in Fig. 3. Alongside, we also plot the corresponding electron density averaged over the same n $\sigma_{x,y}$'s computed using POSINST. For example, electron density and proton density averaged over two $\sigma_{x,y}$'s are, respectively, 2.2×10^{13} and 11.8×10^{13} m^{-3}, implying a neutralization ratio of $r_{\rm neu}\sim 18.7\%$, which is rather appreciable. Here, we must be cautioned that the space-charge tune shift comes from the electric and magnetic parts, which have opposite signs. The electron cloud can only cancel the electric part because it is roughly stationary in the vacuum chamber. Thus the space-charge tune shift is actually reduced by the factor $f_{\rm cl} = \gamma^2[(1-r_{\rm neu})-\beta^2)] = 1-r_{\rm neu}\gamma^2 = 0.584$ at the total energy of 1.4 GeV, where γ and β are the relativistic factors. If we consider the spread of the stability contour in Fig. 1, $(-0.48,-0.18)$, as roughly the spread of the space-charge tune shift, the neutralization by electron cloud will reduce the spread of the stability contour to $(-0.28,-0.105)$. Even if the electron-cloud neutralization were $r_{\rm neu}\sim 30\%$, the spread of the stability contour would be reduced to $(-0.16,-0.060)$. The inductive part of the magnet laminations and connecting beam pipes are found to supply at most an inductive coherent tune shift of ~ -0.04 [2]. Thus there is still no possibility for the coherent tune shift of the beam to be inside the stable region of the stability contour [6]. It is very possible that the neutralization effect of electron-cloud buildup has been overestimated; for example, the SEY can be much less than 1.6. This is because large electron-cloud buildup will signal severe transverse collective beam instabilities and emittance growths in many parts of the booster ramp cycle, especially near the transition energy when the bunch length is shortest [5]. Such severe instabilities and emittance growths have not been reported.

EFFECTS OF BUNCHING

Coasting Beam

The stability contours in Fig. 1 show that a coasting beam has to be unstable if space-charge is large enough. Actually such instabilities have been observed in the Fermilab Recycler Ring [7]. A very long antiproton beam of total length 3.5 μs containing 28×10^{10} particles was cooled stochastically between two barriers to a normalized 95% emittance of $\epsilon_{N95}=3\times10^{-6}$ πm. The synchrotron period is a few seconds. When the vertical chromaticity was reduced

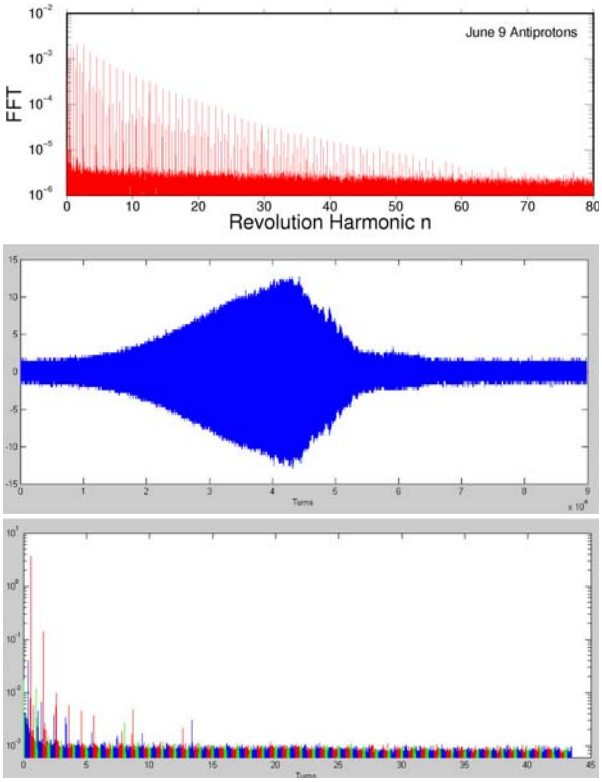

Figure 4: (Color) Top: FFT of difference signals showing an instability of a long $\bar{p}$ beam in the Recycler Ring with slow synchrotron oscillation. Lower: Emittance growth and FFT of difference signals showing an instability of a coasting p beam.

from -2 to 0 to reduce momentum-spread generated Landau damping, the beam became unstable. The difference signals were sampled and their FFT is shown in the upper plot of Fig. 4. The tallest lines are the lower betatron sidebands with the revolution harmonics to the right and upper sidebands to the next right. The excitations roll off very slowly with frequency as if they are driven by the resistive wall impedance. In order to rule out the possibility of two-stream coupled interaction due to trapped ions, the experiment was repeated with a proton beam that could not trap ions. A special proton beam in the Recycler Ring was carefully scraped and debunched to an intensity of 43.9×10^{10} and $\epsilon_{N95} = 6 \times 10^{-6}$ πm. As the chromaticity was reduced from -2 to 0, a vertical instability was observed with a 6-fold increase in emittance blowup. This is depicted together with the FFT of the difference signals in the lower plots of Fig. 4. The observed growth time agrees with computation in the absence of Landau damping. Eventually, a dedicated damper was built to cope with this instability.

Bunched Beam

The situation of a bunched beam can be different. This is because there will be many more particles having

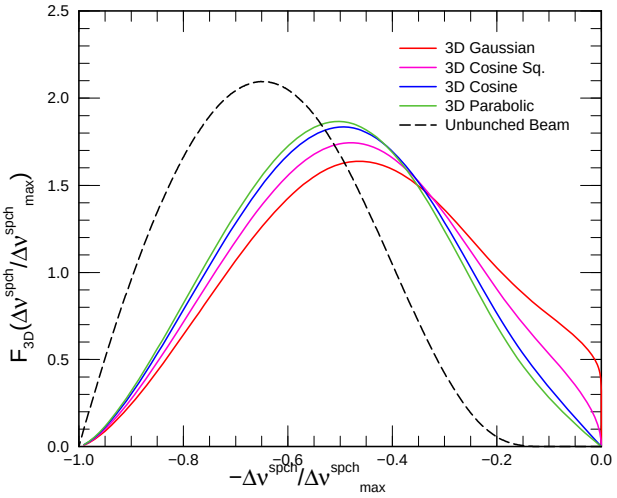

Figure 5: (Color) Plots of distribution in space-charge tune shift in a round bunch with longitudinal Gaussian, cosine square, cosine, and parabolic distribution. The transverse distribution is bi-Gaussian. The distribution of a coasting beam is also shown in dashes for comparison.

smaller space-charge tune shifts, for example, those away from the longitudinal center. Let us first study the distribution of space-charge tune shifts of the particles inside a bunch, which can also shed some light on the shape of the stability contour [4].

The distribution of space-charge tune shift in a coasting beam with circular cross section and bi-Gaussian distribution shows that the distribution is skewed towards higher values, with [8],

$$\frac{\langle \Delta\nu^{\rm spch} \rangle}{\Delta\nu^{\rm spch}_{\rm max}} = 0.6334, \quad \left(\frac{\Delta\nu^{\rm spch}}{\Delta\nu^{\rm spch}_{\rm max}}\right)_{\rm rms} = 0.1678. \quad (4.1)$$

This distribution, called $f_{2D}(\Delta\nu^{\rm spch}/\Delta\nu^{\rm spch}_{\rm max})$, is shown in dashes in Fig. 5. It also shows that the distribution is essentially zero when $\Delta\nu^{\rm spch}/\Delta\nu^{\rm spch}_{\rm max} < 0.15$. This curve has close resemblance to the stability contour in Fig. 1(a). In fact, they should be closely related. For a bunch, however, the space-charge tune shift distribution can be very different because the particles near the two ends have rather small space-charge tune shifts.

Let the longitudinal or linear distribution of the bunch be $\lambda_b(z)$, which is normalized to unity after integrating over z. For a slice of the bunch at z, the number of particles residing in the slice is $N_b\lambda_b(z)dz$. Thus the maximum space-charge tune shift inside this slice is

$$\Delta\nu^{\rm spch}_{\rm max}(z) = \Delta\nu^{\rm spch}_{\rm max}(0)\frac{\lambda_b(z)}{\lambda_b(0)}. \quad (4.2)$$

Here, $\Delta\nu^{\rm spch}_{\rm max}(0)$ is the maximum space-charge tune shift of the whole bunch, and is the same as $\Delta\nu^{\rm spch}_{\rm max}$ in Eq. (4.1)

for the 2D coasting beam. Thus for this particular slice, the distribution in space-charge tune shift is

$$F_{\rm slice}\left(\frac{\Delta\nu^{\rm spch}}{\Delta\nu^{\rm spch}_{\rm max}},z\right)=f_{2D}\left(\frac{\Delta\nu^{\rm spch}\lambda_b(0)}{\Delta\nu^{\rm spch}_{\rm max}\lambda_b(z)}\right)\frac{\lambda_b(0)}{\lambda_b(z)}, \tag{4.3}$$

which is properly normalized that an integration over $\Delta\nu^{\rm spch}/\Delta\nu^{\rm spch}_{\rm max}$ gives unity. The distribution for the whole bunch is therefore

$$\begin{aligned}F_{3D}\left(\frac{\Delta\nu^{\rm spch}}{\Delta\nu^{\rm spch}_{\rm max}}\right)&=\int_{-z}^{z}F_{\rm slice}\left(\frac{\Delta\nu^{\rm spch}}{\Delta\nu^{\rm spch}_{\rm max}},z'\right)\lambda_b(z')dz'\\&=\int_{-z}^{z}f_{2D}\left(\frac{\Delta\nu^{\rm spch}}{\Delta\nu^{\rm spch}_{\rm max}}\frac{\lambda_b(0)}{\lambda_b(z')}\right)\lambda_b(0)dz',\end{aligned} \tag{4.4}$$

where the limits of integration $\pm z$ are given by the excursion of z' at the maximum space-charge tune shift, or $\Delta\nu^{\rm spch}_{\rm max}\lambda_b(z)=\Delta\nu^{\rm spch}\lambda_b(0)$.

Take the Gaussian distribution as an example, the 3D tune-shift distribution is given by

$$F_{3D}\left(\frac{\Delta\nu^{\rm spch}}{\Delta\nu^{\rm spch}_{\rm max}}\right)=\int_{-z}^{z}f_{2D}\left(\frac{\Delta\nu^{\rm spch}}{\Delta\nu^{\rm spch}_{\rm max}}e^{z'^2/2}\right)\frac{dz'}{\sqrt{2\pi}}, \tag{4.5}$$

with $z=\sqrt{-2\ln\left(\Delta\nu^{\rm spch}/\Delta\nu^{\rm spch}_{\rm max}\right)}$. For the cosine square distribution, $\lambda_b(z)=\frac{1}{\hat{z}}\cos^2(\pi z/2\hat{z})$, the 3D tune-shift distribution is

$$F_{3D}\left(\frac{\Delta\nu^{\rm spch}}{\Delta\nu^{\rm spch}_{\rm max}}\right)=\int_{-\theta}^{\theta}f_{2D}\left(\frac{\Delta\nu^{\rm spch}}{\cos^2\theta'\Delta\nu^{\rm spch}_{\rm max}}\right)\frac{2d\theta'}{\pi}, \tag{4.6}$$

with $\theta=\cos^{-1}\sqrt{\Delta\nu^{\rm spch}/\Delta\nu^{\rm spch}_{\rm max}}$. For the cosine distribution, $\lambda_b(z)=(\pi/4\hat{z})\cos(\pi z/2\hat{z})$, the 3D tune-shift distribution is

$$F_{3D}\left(\frac{\Delta\nu^{\rm spch}}{\Delta\nu^{\rm spch}_{\rm max}}\right)=\int_{-\theta}^{\theta}f_{2D}\left(\frac{\Delta\nu^{\rm spch}}{\cos\theta'\Delta\nu^{\rm spch}_{\rm max}}\right)\frac{d\theta'}{2}, \tag{4.7}$$

with $\theta=\cos^{-1}(\Delta\nu^{\rm spch}/\Delta\nu^{\rm spch}_{\rm max})$. Finally, for the parabolic distribution $\lambda_b(z)=\frac{3}{4}(1-z^2/\hat{z}^2)$, the 3D tune-shift distribution is

$$F_{3D}\left(\frac{\Delta\nu^{\rm spch}}{\Delta\nu^{\rm spch}_{\rm max}}\right)=\int_{-z}^{z}f_{2D}\left[\frac{\Delta\nu^{\rm spch}}{(1-z'^2)\Delta\nu^{\rm spch}_{\rm max}}\right]\frac{3dz'}{4}, \tag{4.8}$$

with $z=\sqrt{1-\Delta\nu^{\rm spch}/\Delta\nu^{\rm spch}_{\rm max}}$. These distributions are shown in Fig. 5. These curves show that there are plenty of particles with space-charge tune shift close to zero tune shift, and they are more plentiful when the longitudinal linear density has longer tails. A longitudinal Gaussian distribution may have been too ideal, but the cosine-square distribution is rather realistic. We expect the stability contour for a bunch behaves similarly. As a result, beam stability can be attained provided that there is some reasonable inductive impedance, some extra tune spread arises from octupoles, and $|\,\mathcal{R}e\,Z_1^{\perp}|$ is not too big, while electron cloud need not play an important role.

DISPERSION RELATION OF A BUNCH

The dispersion relation of Métral and Ruggiero for a coasting beam with space-charge and octupole tune spread can be written as

$$1=-\int dJ_x\int dJ_y\frac{J_y\frac{\partial f(J_x,J_y)}{\partial J_y}\left[\Delta\nu^y_{\rm coh}-\Delta\nu^y_{\rm inc}(J_x,J_y)\right]}{\nu_c-\nu_y(J_x,J_y)-m\nu_s}. \tag{5.1}$$

Here, $f(J_x,J_y)$ is the transverse particle density normalized to unity, with $J_{x,y}$ denoting the horizontal and vertical actions of the beam particle. In the denominator, ν_c is the coherent or eigen-betatron tune to be determined, ν_s is the synchrotron tune with spread neglected, m is the azimuthal mode number, and the incoherent tune spread is given by

$$\nu_y(J_x,J_y)=\nu_{y0}(J_x,J_y)+\Delta\nu^y_{\rm inc}(J_x,J_y), \tag{5.2}$$

where $\Delta\nu^y_{\rm inc}$ is the vertical space-charge self-field tune shift, $\nu_{y0}(J_x,J_y)$ is the vertical tune including tune spread coming from octupoles. In the numerator, $\Delta\nu^y_{\rm coh}$ denotes the coherent vertical tune shift driven by impedance.

For a bunch, the above dispersion relation applies to an individual slice at a distance z from the longitudinal bunch center. The dependence on z will appear in the space-charge tune shift $\Delta\nu^y_{\rm inc}$, since the latter is proportional to the linear particle density at z. A simple extension of the dispersion relation to describe a bunch would be an average over the linear particle density $g(z)$, or

$$\begin{aligned}1=&-\int dz\int dJ_x\int dJ_y\times\\&\times g(z)\frac{J_y\frac{\partial f(J_x,J_y)}{\partial J_y}\left[\Delta\nu^y_{\rm coh}-\Delta\nu^y_{\rm inc}(J_x,J_y,z)\right]}{\nu_c-\nu_y(J_x,J_y,z)-m\nu_s},\end{aligned} \tag{5.3}$$

where ν_c now represents the eigen-betatron tune of the whole bunch. A rigorous derivation of this dispersion relation is not available at the moment.

In the model of Métral and Ruggiero, $\nu_{y0}(J_x,J_y)$ is the vertical tune in the presence of octupoles but in the absence of space-charge. It is given by

$$\nu_{y0}(J_x,J_y,z)=\nu_{y00}+aJ_y+bJ_x, \tag{5.4}$$

where ν_{y00} is the bare vertical tune, and

$$a=\frac{3}{8\pi}\int\beta_y^2\frac{\mathcal{O}_s}{B\rho}ds,\ b=-\frac{3}{8\pi}\int 2\beta_x\beta_y\frac{\mathcal{O}_s}{B\rho}ds, \tag{5.5}$$

are the octupole driven tune shifts per unit action, $\mathcal{O}_s$ is the octupole strength, $B\rho$ is the rigidity of the beam, and $\beta_{x,y}$ are the betatron functions. For the vertical incoherent tune shift $\Delta\nu^y_{\rm inc}$, we include only the lowest order of nonlinear space-charge by writing

$$\Delta\nu^y_{\rm inc}(J_x,J_y,z)=\Delta_0(z)+\Delta_a(z)J_y+\Delta_b(z)J_x, \quad (5.6)$$

which is derived by the method of harmonic balance and numerically fitting the space-charge force. Here

$$\Delta_0(z)=\Delta_{00}G(z),\ \Delta_a(z)=\Delta_{a0}G(z),\ \Delta_b(z)=\Delta_{b0}G(z),$$

where $G(z)=2\pi Rg(z)$ is dimensionless playing the role of *local bunching factor*, while Δ_{00}, Δ_{a0}, and Δ_{b0} are the space-charge tune shift and detuning gradients for a coasting beam with the same particle number as the bunch under consideration. Following Métral and Ruggiero, a round beam has been chosen with the transverse particle distribution

$$f(J_x,J_y)=\frac{12}{J^2_{\rm max}}\left(1-\frac{J_x+J_y}{J_{\rm max}}\right)^2, \quad (5.8)$$

so that the dispersion relation can be integrated in the closed form for the transverse coordinates. For this distribution, the maximum action is given by $J_{\rm max}=5\sigma^2$, where σ is the transverse rms beam size. We obtain*

$$\Delta_{a0}=-\frac{9\Delta_{00}}{16J_{\rm max}},\ \Delta_{b0}=-\frac{3\Delta_{00}}{8J_{\rm max}},\ \Delta_{00}=-\frac{N_Br_p}{5\pi\beta\gamma^2\epsilon^{\rm norm}_{\rm rms}}, \quad (5.9)$$

with $\epsilon^{\rm norm}_{\rm rms}$ being the normalized rms emittance.

In the denominator of the integrand in the dispersion relation, the amplitude-dependent tune shifts driven by octupoles and space-charge can be combined to give

$$\nu_y(J_x,J_y,z)=\nu_{y00}+\Delta_0(z)+a_1(z)J_y+b_1(z)J_x. \quad (5.10)$$

with

$$a_1(z)=a+\Delta_a(z) \quad \text{and} \quad b_1(z)=b+\Delta_b(z). \quad (5.11)$$

The denominator can therefore be written as

$$\text{den}=\nu_c-m\nu_s-\nu_{y00}-\Delta_0(z)+S_1(z)\big[j_y+c_1(z)j_x\big], \quad (5.12)$$

where $S_1(z)=-a_1(z)J_{\rm max}$, $c_1(z)=b_1(z)/a_1(z)$, and $j_{x,y}=J_{x,y}/J_{\rm max}$. We next normalize by S_1 and define

$$D(z)=\frac{\text{den}}{S_1(z)}=\frac{q_c-\Delta_0(z)}{S_1(z)}+j_y+c_1(z)j_x, \quad (5.13)$$

where $q_c=\nu_c-m\nu_s-\nu_{y00}$ plays the role of the coherent (or eigen-) transverse oscillation frequency to be determined from the dispersion.

The numerator of the integrand in Eq. (5.3) is

$$\begin{aligned} J_y\frac{\partial f(J_x,J_y)}{\partial J_y}&\Big[\Delta\nu^y_{\rm coh}-\Delta\nu^y_{\rm inc}(J_x,J_y,z)\Big]\\ &=-\frac{24}{J^2_{\rm max}}(1-j_x-j_y)\times\\ &\quad\times\Big[\Delta\nu^y_{\rm coh}-\Delta_0(z)-\Delta_a(z)j_y-\Delta_b(z)j_x\Big]. \quad (5.14)\end{aligned}$$

*We did not do the actual fitting to the space-charge force. The fitting was approximated by including an extra factor of $\frac{1}{2}$ in Δ_{a0} and Δ_{b0}.

The merit of the Métral and Ruggiero model is that the transverse coordinates can be integrated analytically, thus leaving only one numerical integration to perform for the longitudinal coordinate. After the integration over j_x and j_y are performed, the dispersion relation becomes

$$\begin{aligned}1=\int dz\frac{24g(z)}{S_1(z)}\Big\{&\Big[\Delta Q^y_{\rm coh}-\Delta_0(z)\Big]I_1-\\ &-J_{\rm max}\Big[\Delta_a(z)I_2+\Delta_bI_3\Big]\Big\}, \quad (5.15)\end{aligned}$$

where the analytic closed forms

$$I_i(z)=\int_{j_y=0}^1 dj_y\int_{j_x=0}^{1-j_y}dj_x\frac{p_i(1-j_x-j_y)}{D(z)}, \quad (5.16)$$

with $p_1=j_y$, $p_2=j_y^2$, $p_3=j_xj_y$, are depicted in the Appendix. With the further definition

$$\begin{aligned}K_1&=\int dz\,I_1(z)\frac{g(z)}{S_1(z)},\\ K_{23}&=\int dz\Big\{J_{\rm max}\Big[\Delta_a(z)I_2(z)+\Delta_b(z)I_3(z)\Big]+\\ &\quad+\Delta_0(z)I_1(z)\Big\}\frac{g(z)}{S_1(z)}, \quad (5.17)\end{aligned}$$

the dispersion relation reduces to

$$\Delta\nu^y_{\rm coh}=\frac{1}{K_1}\left[\frac{1}{24}+K_{23}\right]. \quad (5.18)$$

Numerical Solution

As in all dispersion computation, we apply various real values to the eigen-tune ν_c (actually q_c) in the denominator of the integrand of Eq. (5.3) with an infinitesimal negative imaginary part to obtain the corresponding $\Delta\nu^y_{\rm coh}$'s of Eq. (5.18). The final integration over z is performed numerically. The plot of $\mathcal{R}e\,\Delta\nu^y_{\rm coh}$ versus $\mathcal{I}m\,\Delta\nu^y_{\rm coh}$ gives the stability contour of the dispersion relation.

We choose the generalized elliptical distribution

$$g(z)=\frac{A_n}{\hat{z}}\left(1-\frac{z^2}{\hat{z}^2}\right)^n \quad \text{for } |z|\le\hat{z}, \quad (5.19)$$

as the longitudinal linear distribution of the bunch with $A_n=\Gamma(n+\frac{3}{2})/[\sqrt{\pi}\,\Gamma(n+1)]$ for any $n>-1$, where $g(z)$ is normalized to unity when integrated over z. Note that n need not be an integer or half integer. The rms bunch length is given by $\sigma_z^2=\hat{z}^2/(2n+3)$. The merit of this distribution is that it begins with the parabolic distribution when $n=1$ and beam tails become lengthened when n increases. It finally approaches the Gaussian distribution when $n\to\infty$.

The stability contours for various values of n are shown in Fig. 6. The stability contour for octupoles that

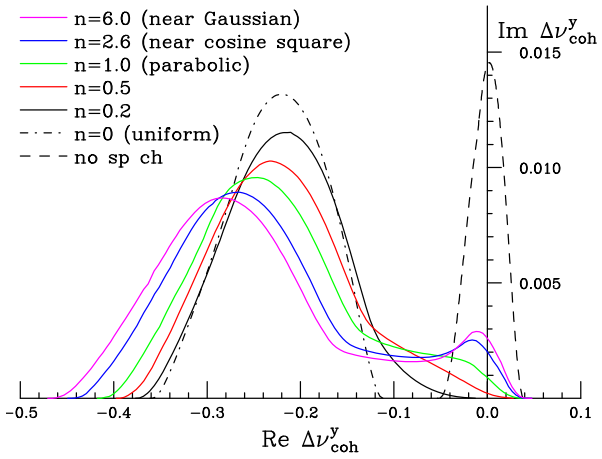

Figure 6: (Color) Stability contours for various longitudinal generalized elliptical bunch distributions, from $n = 0$, the uniform distribution, to $n = 1/2$, the elliptical distribution, to $n = 1$, the parabolic distribution, to $n = 2.6$, roughly the cosine square distribution, and to $n = 6$, roughly the Gaussian distribution. It is clear that as n increases the stability contour spreads out more and more reaching and eventually covering $\mathcal{R}e\,\Delta\nu^y_{\rm coh} = 0$, thus providing Landau damping if $|\,\mathcal{R}e\,Z_1^\perp|$ is not too large. The stability contour for octupole alone without space-charge is also shown in dashes.

contribute tune spreads of $-0.042 < \Delta\nu_y < 0.065$ in the absence of the space-charge force is plotted in dashes. With the space-charge force turned on (the octupole detuning per horizontal action in the same direction as the space-charge detuning), the longitudinal linear particle distribution is varied from $n = 0$ to $n = 6$, while the rms bunch length is kept fixed at $\sigma_z = 0.70$ m all the time. Here $n = 0$ corresponds to the uniform distribution and its stability contour† (dot-dash) is far from the $\mathcal{R}e\,\Delta\nu^y_{\rm coh} = 0$ point. As n increases, the stability contour spreads out. Even for $n = 1$ (green), the parabolic distribution, the stability curve covers the $\mathcal{R}e\,\Delta\nu^y_{\rm coh} = 0$ point already, implying that there can be Landau damping if the real part of the transverse impedance $|\,\mathcal{R}e\,Z_1^\perp|$ is small enough, even when there is no inductive contribution from the vacuum chamber. When n increases to 2.6 (blue), which is roughly the cosine square distribution, the stability contour exhibits a small bump near $\mathcal{R}e\,\Delta\nu^y_{\rm coh} = 0$. The spread of the stability curve does not increase by much even when $n = 6$ (magenta), which is close to the Gaussian distribution.

Some comments are in order. First, the stability limit appears to be $\mathcal{I}m\,\Delta\nu^y_{\rm coh} \sim 0.002$ and is roughly independent of the longitudinal distribution when the distribution spreads out more than parabolic. Second, this limit appears to be small but without Landau damping it corresponds to a growth time of 0.17 ms which is rather short. Third, we require here an octupole tune spread of the order of 0.05 to generate this amount of stability limit, implying that the spread of synchrotron tune, if included, may not be significant here. Fourth, this stability limit decreases rapidly with the decrease in octupole tune spread. For example, 70% of the present octupole tune spread will lower the stability limit $\mathcal{I}m\,\Delta\nu^y_{\rm coh}$ by one order of magnitude.

†This corresponds to a bunch with uniform linear distribution with half bunch length equal $\sqrt{3}\,\sigma_z$. The stability contour is different from that in Fig. 1, where the maximum possible space-charge has been assumed by using the bunching factor of a Gaussian bunch.

APPLICATION TO FERMILAB BOOSTER NEAR INJECTION

Coherent Tune Shift and Coupling Impedance

From Sacherer's integral equation, the coherent tune shift $\Delta\nu^y_{\rm coh}$ can be solved as a function of the transverse coupling impedance $Z_1^\perp$. To the lowest order of approximation without azimuthal mode coupling, the vertical coherent tune shift for the mth azimuthal mode and kth radial mode of the μth coupled-bunch mode of M equally spaced bunches each containing N_b particles is given by

$$\left[\Delta\nu^y_{\rm coh}\right]_{\mu mk} = -i\frac{r_p N_b}{2\pi\gamma\nu_y Z_0} Z_1^\perp\Big|^{\mu mk}_{\rm eff} \qquad (6.1)$$

where

$$Z_1^\perp\Big|^{\mu mk}_{\rm eff} = \frac{M}{\bar\beta_y}\sum_q \left[\beta_y Z_1^\perp(\omega_q)\right]\left|\tilde\lambda_{mk}(\omega_q-\omega_\xi)\right|^2, \qquad (6.2)$$

with $\omega_q/\omega_0 = qM+\mu+\nu_y+m\nu_s$, ω_0 being the angular revolution frequency, q any integer, ν_y the vertical betatron tune, $\omega_\xi = \xi_y\omega_0/\eta$ the chromatic frequency shift, ξ_y the vertical chromaticity, and η the slip factor. The notation $\left[\beta_y Z_1^\perp(\omega_q)\right]/\bar\beta_y$ implies that the transverse impedance $Z_1^\perp$ should be summed up item-by-item along the vacuum chamber with $\beta_y/\bar\beta_y$ acting as a weight, where β_y is the local betatron function and $\bar\beta_y = R/\nu_y$ is the mean along the ring. In our discussion, the impedance comes mostly from the wall of the vacuum chamber and the weighted summation is therefore not necessary. The other variables are $Z_0 \approx 376.7\ \Omega$ the free-space impedance, and $\tilde\lambda_{mk}$ the spectrum of the linear distribution of excitation of the mth azimuthal and kth radial mode. For the Gaussian linear distribution [10],

$$\tilde\lambda_{mk}(\omega_n) = i^{-(m+2k)}\sqrt{\frac{1}{k!(m+k)!}}\left[\frac{\omega_n\sigma_\tau}{\sqrt{2}}\right]^{m+2k} e^{-\frac{1}{2}\omega_n^2\sigma_\tau^2}, \qquad (6.3)$$

where $\sigma_\tau = \sigma_z/(\beta c)$ is the rms bunch length in time, with c being the velocity of light.

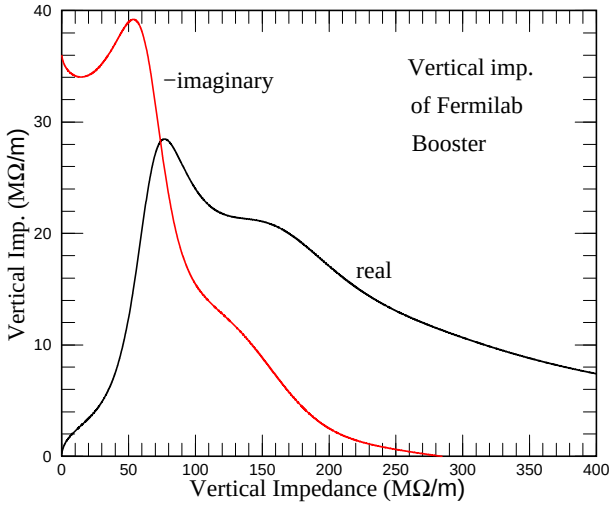

Figure 7: (Color) Vertical dipole impedance of the Fermilab Booster laminated magnets computed by approximating the magnet gap by parallel surfaces. The contribution of the beam pipes joining the magnets is too small to be seen.

We see that, because of the spectral content of the bunch, one value of the eigen-tune ν_c in the dispersion function corresponds to a weighted combination of transverse impedance at various frequencies, but only one value of the coherent tune shift $\Delta\nu^y_{\rm coh}$. This explains why the stability plot is depicted in the complex plane of the coherent tune shift instead of that of the transverse impedance.

Coupled-Bunch Instabilities

Protons are injected from a linac into the Fermilab Booster at the kinetic energy of 400 MeV and are then captured adiabatically into $M = 84$ equally spaced bunches each containing $N_b = 6\times10^{10}$ protons. The space-charge force is actually at a maximum slightly into the ramp cycle when the bunch length becomes shorter. Here we study the situation when the total particle energy becomes $E = 1.40$ GeV and rms bunch length $\sigma_z = 0.70$ m or $\sigma_\tau = 3.15$ ns. The transition gamma of the Booster is $\gamma_t = 5.446$ so that the slip factor is $\eta = -0.4154$. Since the magnets are unshielded and the beam sees the magnet laminations, the coupling impedance is dominated by the contribution from the laminated walls. The transverse impedance of the laminated magnet surfaces have been computed approximately using the method of surface impedance per square and the method of equivalent transverse propagation constant [9]. The openings of these combined-function magnets are approximated by parallel laminated surfaces and the computed impedance is depicted in Fig. 7. Notice that because of the large value of the lamination impedance, $\mathcal{R}e\, Z_1^\perp$ bends back to zero below ~ 75 MHz. As a result, the laminations, although very resistive, contribute little to coupled-bunch instabilities.

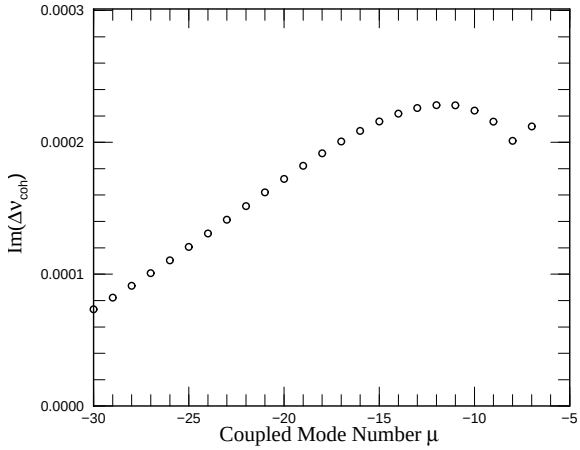

Figure 8: $\mathcal{I}m\,\Delta\nu^y_{\rm coh}$ for the most unstable coupled bunch mode μ. Note that the most unstable one is slightly away from the $(1-Q)$ mode at $\mu=-7$ due to finite lamination contribution.

The stainless steel beam pipes joining the magnets produce a vertical impedance of

$$\mathcal{R}e\, Z_1^\perp\Big|_{\rm pipe}(\omega) = \big[\,{\rm sgn}(\omega) - i\big]\frac{0.199}{\sqrt{|\omega/\omega_0|}}\ {\rm M\Omega/m}, \quad (6.4)$$

which is too small to be visible if plotted together with the lamination contributions in Fig. 7. However, because these pipe contributions are small, $\mathcal{R}e\, Z_1^\perp\big|_{\rm pipe}$ bends back to zero at the very low frequency, ~ 100 Hz, and $\big|\mathcal{I}m\, Z_1^\perp\big|_{\rm pipe,max} = 12.9$ MΩ/m. Thus the pipe contribution may overtake the lamination contribution at low frequencies and becomes the dominating driving force of coupled-bunch instabilities. In fact, at the $(1-Q)$ line, $(\omega/\omega_0 = -0.2)$, $\mathcal{R}e\, Z_1^\perp\big|_{\rm pipe} = -0.43$ MΩ/m while $\mathcal{R}e\, Z_1^\perp\big|_{\rm lamination} = -0.24$ MΩ/m. As a result, the contribution of the lamination can also be important. We computed the effective transverse impedance at various coupled modes μ, according to Eq. (6.2) including both the lamination and beam pipe contributions, while keeping the chromaticity $\xi_y = 0$. For the azimuthal mode $mk = (0,0)$, the imaginary parts of the coherent tune shifts corresponding to the most unstable coupled-bunch modes are plotted in Fig. 8. We see that the most unstable mode is $\mu = -12$ and the coherent tune shift is $\Delta\nu^y_{\rm coh} = -0.0257 + i0.000228$, which would amount to a growth time of 1.49 ms in the absence of Landau damping. With the presence of octupoles, it is clear that this coherent tune shift is well within the stability region for Gaussian linear distribution in Fig. 6. Thus all coupled-modes are stable when octupoles contribute a tune spread of $-0.042 < \Delta\nu_y < 0.065$.

Single-Bunch Head-Tail Instabilities

In the study of single-bunch instability, we substitute $M = 1$ in the effective impedance of Eq. (6.2). Unlike the situation of coupled-bunch calculation, now the summation is over every harmonic with the excitation mode power spectrum as weight factor. Here, the impedance contribution is completely dominated by the laminations of the magnets while that of the beam pipes plays negligible role. This is because the beam pipes cover only $\sim 40\%$ of the vacuum chamber and these pipes are of rather large transverse dimension so as to accommodate the space-charge dominated beam at low energies. We can therefore model the transverse impedance of the Fermilab Booster as a broad-band resonance centered at $f_r \sim 85$ MHz.

With the neglect of mode-coupling, we need to consider only the most prominent radial mode $k = 0$. The azimuthal mode $m = 0$ is the one that is most easily subject to instability because of its relatively large power spectrum. This mode is most unstable when the mode spectrum is shifted towards the peak of the broad-band resonance at negative frequency (see Fig. 9). This requires a chromaticity of $\xi_y = -\eta f_r/f_0 \sim 75$, where $f_0 = \omega_0/(2\pi)$. Detailed numerical summation of the effective impedance gives $\xi_y = +99$, at which $\Delta\nu^y_{\rm coh} = -0.012 + i0.016$, which is too large to be Landau damped according to the stability plot of Fig. 6. However, this is of no alarm, because it is not possible to operate the Fermilab Booster at such high chromaticity; the vertical bare tune is only $\nu_y \approx 6.8$ and the maximum momentum spread is $\sim \pm 1\%$. The operational

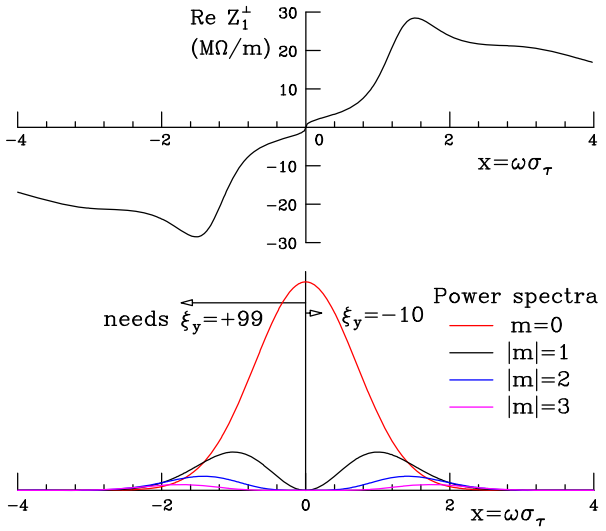

Figure 9: Plot showing shifts of power spectra of azimuthal modes under chromaticity ξ_y along the frequency axis with respect to the transverse impedance $\mathcal{R}e\, Z_1^\perp$.

chromaticity is usually at most $\xi_y \sim \pm 10$. Even at $\xi_y = 10$, the coherent tune shift is $\Delta\nu^y_{\rm coh} = -0.255 + i0.0022$, which is close to the stability boundary. Most of the time, the Fermilab Booster runs at negative chromaticity near injection, so as to guarantee stability of this $m = 0$ head-tail mode. It is important to point out that the Fermilab Booster is a fast ramping machine at 15 Hz, so a slight instability in a small energy range is of no significance, because very soon the beam particles will be at much higher energies and the space-charge force will decrease accordingly.

To study other head-tail modes, it is most convenient to consider the variable $\omega\sigma_\tau$. We learn from Eq. (6.3) that the power spectrum of the mth azimuthal mode peaks at $\omega\sigma_\tau = \sqrt{|m|}$. The peak of the broad-band resonance of the lamination impedance at $f_r \sim 85$ MHz corresponds to $\omega_r\sigma_\tau \sim 1.7$. Thus the peaks of azimuthal excitations with $|m| = 0$, 1, 2 are of lower frequency than the resonance peak, the peak of the $|m| = 3$ mode excitation is roughly on top of the lamination resonance peak, while those with $|m| > 3$ lie on the two higher-frequency sides (see Fig. 9). When the chromaticity becomes negative, all azimuthal modes have their spectra shifted to the right towards higher frequencies, since we are well below transition. Modes $|m| = 0$, 1, 2, 3 will sample more impedance at positive frequencies and less impedance at negative frequencies and are therefore stable. The spectra of modes $|m| \geq 4$ sample more impedance at negative frequencies and are therefore unstable. Mode $|m| = 4$ will become most unstable when the peak of its power spectrum is moved by chromaticity to the peak of the resonance impedance. The amount of chromaticity required to do so is given by $\xi_y\omega_0\sigma_\tau/\eta \sim \sqrt{4} - \sqrt{3}$, or $\xi_y \sim -12$. Detailed numerical computation gives $\xi_y = -15$ at which $\mathcal{I}m\,\Delta\nu^y_{\rm coh} = 0.000052$, which is not far from our estimation, remembering that the lamination resonance impedance is not a well-behaved symmetric resonance but has long high-frequency tails. This value of $\mathcal{I}m\,\Delta\nu^y_{\rm coh}$ is well within the stability region provided by the stability contour in Fig. 6; the mode is therefore stable. The smallness of $\mathcal{I}m\,\Delta\nu^y_{\rm coh}$ comes about because the peak value of the $|m|$th mode power spectrum decreases roughly as $e^{-|m|}$. This decrease will not be as much if the longitudinal linear distribution is not Gaussian, but with shorter tails. For example, if we consider instead the approximated Sacherer sinusoidal modes, the peaks of the corresponding azimuthal modes are all separated by $\Delta\omega \sim \pi/(4\sigma_\tau)$, much farther apart than the Hermite modes of the Gaussian distribution,

where the total bunch length is assumed to be $4\sigma_\tau$. Then, to shift one azimuthal mode to the position of the consecutive mode will require a chromaticity of $\xi_y = \pi\eta/(4\omega_0\sigma_\tau)$, which is about three times as much as for the Hermite modes. Such large chromaticity is far from the operational chromaticity of the Fermilab Booster. Numerical computation shows that even up to $\xi_y = -15$, the most unstable mode is $|m| = 4$ with $\mathcal{I}m\,\Delta\nu^y_{\rm coh} = 0.00082$, still below the stability limit. In short, the head-tail modes should all be stable if the chromaticity is negative and less than ~ 10 units. One important reason behind this conclusion is the relatively large slip factor near injection ($\eta = -0.4154$), which makes chromaticity inefficient in shifting the power spectra along the frequency axis. This explains why the Fermilab Booster can often run at the *wrong* chromaticity (or positive chromaticity) near injection. This will no longer be true when the beam energy reaches transition. Near transition $|\eta|$ is small and even a small chromaticity can shift the power spectra of the azimuthal modes by a large amount. Luckily, the space-charge force at those energies will become much less, as will its effects on the stability contours.

CONCLUSION

The dispersion relation of Métral and Ruggiero in the presence of octupole tune spread and space-charge force has been extended to that for a bunch. The integration is performed analytically in the two transverse dimensions and numerically in the longitudinal dimension, resulting in the stability contour in the complex coherent-tune-shift plane. A wide range of longitudinal linear distributions, from uniform to parabolic and Gaussian, have been considered, and their stability contours compared. The result shows that there will be finite Landau damping provided that the longitudinal distribution spreads out on both sides more than the parabolic distribution.

The stability contour corresponding to the longitudinal Gaussian distribution is applied to the Fermilab Booster near injection when the total particle energy is of 1.40 GeV. First, we look into transverse coupled bunch instabilities for a full ring of 84 equally space bunches. The coherent tune shift is computed according to the impedance of the unshielded laminated magnets and the beam pipes joining them together. We find that for the azimuthal mode $m = 0$, $\mathcal{I}m\,\Delta\nu^y_{\rm coh}$'s of all coupled-bunch modes are well within the stable region of the stability contour. Without Landau damping, the most unstable mode will have a growth time of ~ 1.5 ms. In the analysis, we assume octupoles supplying action dependent tune spreads of $-0.042 < \Delta\nu_y < 0.065$ in the same direction as the gradient of the space-charge detuning. Actually, all these coupled modes remain stable even if the octupole strength is reduced by one half. Next, the single-bunch head-tail modes are studied. The worst situation is when the $m = 0$ mode is shifted by chromaticity towards the resonance peak of the approximated broad-band impedance of the laminated magnets. This mode will become unstable when $\xi_y \gtrsim 10$, which is outside the operation range of the machine. With $\xi_y < 0$, modes $m = 0$, ±1, ±2, and ±3 are stable while modes $|m| \geq 4$ are unstable if there is no octupole damping at all. However, $\mathcal{I}m\,\Delta\nu^y_{\rm coh}$'s are small for these modes and all of them are well inside the stable region of the stability plot. This happens because, first, the magnitudes of their power spectra roll off according to $e^{-|m|}$, and second, the relatively large slip factor near injection makes the shifting of power spectra by chromaticity along the frequency axis very inefficient.

In short, we now understand how octupole tune spread can provide Landau damping to a bunch with strong space-charge, like the ones in the Fermilab Booster, although such Landau damping may not be possible for a coasting beam or a bunch with uniform longitudinal distribution. There are two issues that have not been answered. First, only non-coupled azimuthal and radial modes have been considered. When these modes couple, the spread in synchrotron tune in the dispersion relation may become important and cannot be ignored. The dispersion relation for a bunch, Eq. (5.3), is merely a suggestion of the extension from that for a coasting beam. Its rigorous derivation is still unavailable at the moment.

APPENDIX

Let $q(z) = [q_c - \Delta_0(z)]/S_1(z)$, where $q_c = \nu_c - m\nu_s - \nu_{y00}$ and ν_c is the eigen-tune of the dispersion relation. Then $I_1(z)$, $I_2(z)$, and $I_3(z)$ are exactly the same integrals discussed by Métral and Ruggiero [1]. In the closed form in terms of $q(z)$ and $c_1(z)$, these integrals give the following expressions [11]:

$$I_1 = -\frac{1}{6c_1^2(c_1-1)^2}\Big\{c_1(c_1-1)\big[q^2(2c_1-1)+2qc_1+c_1\big]+ \\ +(q+c_1)^3\ln\frac{q+1}{q+c_1}- \\ -(c_1-1)^2q^2\big[q(2c_1+1)+3c_1\big]\ln\frac{q+1}{q}\Big\}, \qquad \text{(A.1)}$$

$$I_2 = +\frac{1}{24c_1^2(c_1-1)^3}\Big\{c_1(c_1-1)\big[2q^3(3c_1^2-5c_1+1)+ \\ +q^2c_1(5c_1-11)-2qc_1(c_1+2)-c_1(3c_1-1)\big]- \\ -2(q+c_1)^4\ln\frac{q+1}{q+c_1}- \\ -2(c_1-1)^3q^3\big[q(3c_1+1)+4c_1\big]\ln\frac{q+1}{q}\Big\}, \quad \text{(A.2)}$$

$$I_3 = +\frac{1}{24c_1^3(c_1-1)^3}\Big\{c_1(c_1-1)\big[2q^3(c_1^2-c_1+1)+ \\ +3q^2c_1(c_1+1)+6qc_1^2+c_1^2(c_1+1)\big]+ \\ +2(q+c_1)^3\big[q(2c_1-1)+c_1\big]\ln\frac{q+1}{q+c_1}- \\ -2(c_1-1)^3q^3\big[q(c_1+1)+2c_1\big]\ln\frac{q+1}{q}\Big\}. \quad \text{(A.3)}$$

They are all complex variables. Their imaginary parts come from the logarithmic terms. Their values are determined as follows according to the variable a_1, the combined tune shift gradient of the octupole and the transverse space-charge force defined in Eqs. (5.4), (5.6), and (5.11). For the stability contour, the imaginary part is introduced by letting

$$q \to q \pm i\epsilon \qquad \text{for } a_1 \gtrless 0, \quad \text{(A.4)}$$

with ϵ being an infinitesimally small positive number. The result turns out to be,

for $a_1 > 0$,

$$\ln\frac{q+1}{q} = \ln\left|\frac{q+1}{q}\right| + i\begin{cases} 0 & q(q+1)>0, \\ -\pi & q(q+1)<0, \end{cases}$$

$$\ln\frac{q+1}{q+c_1} = \ln\left|\frac{q+1}{q+c_1}\right| + i\begin{cases} 0 & (q+1)(q+c_1)>0, \\ \pm\pi & \begin{cases}(c_1-1)\gtrless 0 \text{ and} \\ (q+1)(q+c_1)<0,\end{cases}\end{cases}$$

for $a_1 < 0$,

$$\ln\frac{q+1}{q} = \ln\left|\frac{q+1}{q}\right| + i\begin{cases} 0 & q(q+1)>0, \\ +\pi & q(q+1)<0, \end{cases}$$

$$\ln\frac{q+1}{q+c_1} = \ln\left|\frac{q+1}{q+c_1}\right| + i\begin{cases} 0 & (q+1)(q+c_1)>0, \\ \pm\pi & \begin{cases}(c_1-1)\lessgtr 0 \text{ and} \\ (q+1)(q+c_1)<0.\end{cases}\end{cases} \quad \text{(A.5)}$$

REFERENCES

[1] E. Métral and F. Ruggiero, *Stability diagrams for Landau damping with two-dimensional betatron tune spread from both octupoles and non-linear space charge*, CERN-AB-2004-025 (ABP), 2004.

[2] Xiaobiao Huang, *Beam Diagnosis and Lattice Modeling of the Fermilab Booster*, PhD thesis, Indiana University, 2005.

[3] M.A. Furman and G.R. Lambertson, *The Electron-Cloud Instability in the Arcs of the PEP-II Positron Ring*, LBNL Report LBNL-441123/CBP Notes-246, PEP-II AP Note AP 97.27, Proc. Int. Workshop on Multibunch Instabilities in Future Electron and Positron Accelerators (MBI-97), ed. Y.H. Chin, KEK, Tsukuba, Japan, July 15–18, 1997; M. A. Furman, *The Electron-Cloud Effect in the Arcs of the LHC*, LBNL Report LBNL-41482/CBP Note 247/LHC Project Report 180, May 20, 1998.

[4] K.Y. Ng, *Electron Cloud in the Fermilab Booster*, PAC'07, 2007, p.3895; *Electron Cloud and Space-Charge Effects in the Fermilab Booster*, FERMILAB-FN-0803-AD, 2007.

[5] K.Y. Ng, *Analysis of Possible Electron-Cloud Induced Collective Instabilities in the Fermilab Booster*, Fermilab Report FERMILAB-FN-0806-AD, 2007.

[6] At SEP= 1.6, electron cloud reaches saturation only inside the D-magnets and the beam pipes ($\sim 70\%$ of the ring) but not inside the F-magnets, which have larger aperture. Thus the neutralization factor of $r_{\rm neu} = 0.187$ inside the D-magnets and the beam pipes is equivalent to an average neutralization factor of $\bar{r}_{\rm neu} = 0.131$ for the whole ring or a space-charge reduction factor of $f_{\rm cl} = 0.709$. The stability contour is then shifted to $(-0.34, -0.128)$. For $r_{\rm neu} = 0.30$, $\bar{r}_{\rm neu} = 0.21$ and $f_{\rm cl} = 0.532$. The stability contour is shifted to $(-0.26, -0.096)$.

[7] K.Y. Ng, *Resistive-Wall Instability at Fermilab Recycler Ring*, ICFA-HB2004 Workshop, Bensheim, Germany, 2004; *Transverse Instability at the Recycler Ring* Fermilab Report FERMILAB-FN-0760-AD, 2004.

[8] See for example, K. Y.Ng, *Distribution of Incoherent Space-Charge Tune Shift of a Bi-Gaussian Beam*, Fermilab Report TM-2241, 2004.

[9] K.Y. Ng, *Coupling Impedance of Laminated Magnets*, Fermilab Report FN-0744, 2004.

[10] These are the so-called Hermite modes. See for example, K.Y. Ng, *Physics of Intensity Dependent Beam Instabilities*, World Scientific, p. 374. There, the $\sqrt{2\pi}$ in the denominator has been moved to the factor before $Z_1^{\perp}\big|_{\rm eff}$.

[11] The expressions for I_1, I_2, and I_3 are exactly the same for K_1, K_2, and K_2 in Eqs. (29) to (31) of Métral and Ruggiero [1]. They are reproduced here because there are typos in the latter.